galaxies

IMPACT FACTOR 3.2

CITESCORE 4.9

Review

Quantum Technologies for the Einstein Telescope

Mikhail Korobko

Special Issue

Challenges for Third-Generation Gravitational Wave Detectors and Beyond

Edited by

Dr. Annalisa Allocca, Dr. Lucia Trozzo and Dr. Valeria Sequino

MDPI

https://doi.org/10.3390/galaxies13010011

galaxies

MDPI

Review

Quantum Technologies for the Einstein Telescope

Mikhail Korobko

Institut für Quantenphysik and Zentrum für Optische Quantentechnologien, Universität Hamburg, Luruper Chaussee 149, 22761 Hamburg, Germany; mikhail.korobko@uni-hamburg.de

Abstract: Quantum technology is central to the operation of modern gravitational-wave detectors and will play crucial role in the success of next-generation observatories, such as the Einstein Telescope. There, quantum squeezed light will be utilized to suppress quantum noise across the entire detection band, a task that demands advancements in several areas of quantum technology. This review provides an introduction to the quantum technologies employed in gravitational-wave detection and explores in detail their properties, challenges, and the potential they hold for the Einstein Telescope.

Keywords: quantum technology; squeezed light; gravitational-wave detection

1. Introduction

The spectacular success of modern gravitational-wave (GW) detectors, Advanced LIGO [1], Advanced Virgo [2], GEO600 [3], and KAGRA [4], has launched a new era of astronomy and astrophysics, allowing us to observe phenomena like black hole mergers [5–9] and neutron star collisions [10–12]. This success is enabled by the unprecedented measurement precision of the detectors, where quantum technology lies at the very heart of the experimental design. Among many noises that limit the sensitivity of the detectors, quantum noise is currently one of the primary obstacles to improving the detector sensitivity [13–17]. Quantum noise arises from the quantum nature of light and its interaction with mirrors. It manifests in two forms: shot noise (SN), which dominates at high frequencies due to the quantum uncertainty in the amount of photons reaching the photodetector per time interval, and quantum radiation pressure noise (QRPN), which dominates at low frequencies due to quantum fluctuations in the force exerted by photons on mirrors [18–20]. Together, these two effects limit the sensitivity of interferometric detectors across most of their detection band [14].

The need to suppress quantum noise has been driving the development of advanced quantum technologies, most notably the use of squeezed light [21–25]. The squeezed light technology for GW detection was researched and developed between 2002 and 2010 (for a review, see Ref. [26]). Since its first permanent installation and operation in a large-scale detector in 2010 [27–29], quantum squeezed light has become an indispensable tool for GW detection. Squeezing reduces quantum uncertainty in one observable (e.g., the phase quadrature of the light field) at the expense of increased uncertainty in its conjugate (correspondingly the amplitude quadrature), allowing detectors to selectively suppress either SN or QRPN [23,30]. By 2019, both Advanced LIGO and Advanced Virgo had incorporated quantum squeezing into their operations [15,16], significantly enhancing their sensitivity. All GW merger events since then had been detected in a quantum enhanced detector [9]. In 2021, GEO600 became the first large-scale facility to reach the landmark value of 6 dB of quantum noise reduction [31]. In 2023, Advanced LIGO further advanced

Academic Editor: Annalisa Allocca

Received: 15 December 2024
Revised: 24 January 2025
Accepted: 1 February 2025
Published: 5 February 2025

Citation: Korobko, M. Quantum Technologies for the Einstein Telescope. *Galaxies* **2025**, *13*, 11. https://doi.org/10.3390/galaxies13010011

this technology by deploying frequency-dependent squeezing [32,33], which suppresses both SN and QRPN simultaneously in a broad frequency band [20,34,35].

As GW observatories move toward next-generation facilities like the Einstein Telescope (ET) [36,37] and Cosmic Explorer (CE) [38–41], quantum noise suppression will remain a cornerstone technology. Pushing the sensitivity of the detectors by a factor of 10 across the full spectrum will require even more sophisticated quantum enhancements to detect faint signals from previously inaccessible GW sources, such as primordial black holes [42] or the stochastic GW background [43], or studying parameter and populations of known sources [36,44–49]. As we explore in this review, the ET in particular, due to its unique design, presents new challenges for quantum noise suppression, demanding innovations that extend beyond the current state of the art.

The ET, planned for construction in Europe with an expected launch by the mid-to-late 2030s, will incorporate the most advanced technologies to address fundamental and technical noise sources [37,50]. To reduce the impact of seismic and Newtonian seismic noise, the facility will be located several hundred meters underground [51–53]. One of the ET's standout features is its "xylophone" configuration, where two specialized detectors are optimized for different frequency ranges [54]; see Figure 1. The low-frequency (LF) detector will target 2–30 Hz, while the high-frequency (HF) detector will cover 30 Hz to 3 kHz. The LF detector will employ cryogenic cooling to suppress low-frequency thermal noise in mirrors and suspension [55–57]. To make the detector compatible with cryogenics, it will also use low optical power in the arms: only 18 kW (compared, e.g., to the design value of 750 kW in Advanced LIGO) and 1550 nm wavelength to enable the use of low-loss mirror substrates and coatings [58,59]. The HF detector, on the contrary, will feature very high power inside the arms, up to 3 MW, at a wavelength of 1064 nm. Together, the combined output of LF and HF detectors will achieve a broadband sensitivity that exceeds the capabilities of current detectors by a factor of ≈10, also moving towards lower frequencies, opening the way for especially interesting astrophysical observations [36]. The ET may adopt either a triangular configuration, with three pairs of interferometers with central beam-splitters located at the vertices, or a more traditional L-shaped design with detector pairs at separate locations [49].

Both the LF and the HF detectors will be limited by quantum noise across most of their frequency bands, although they face distinct challenges in quantum noise suppression. These differences arise from their specific optical linewidths, arm power levels, and operational tuning. For example, the LF detector will operate detuned from resonance, adding additional complexity to noise suppression strategies [50]. The ET targets several critical frequency ranges that promise to enable novel observations. These frequencies are primarily limited by quantum noise, making effective quantum noise mitigation central for the observatory's success. Of particular importance is the frequency range around 8 Hz in the ET-LF, where the detector reaches its highest sensitivity by employing the optical spring approach. This sensitivity will play a key role in achieving a high observational reach [60], improving source localization for multi-messenger follow-up campaigns [61], and detecting faint, previously inaccessible sources such as primordial black holes [62]. Another significant frequency range lies above 1 kHz, where the ET-HF is expected to observe post-merger effects. These observations will provide crucial insights into the equation of state of ultra-dense quantum matter in neutron stars [63] and allow tests for deviations from general relativity in the post-merger oscillations of black holes [64,65], among other interesting phenomena [36].

This review is structured in the following way: first, we give a brief overview of quantum noise in GW detectors; then, we go into detail on the planned quantum technol-

ogy for the ET, the challenges associated with quantum noise, and potential alternative configurations; and finally, we conclude with a discussion and outlook.

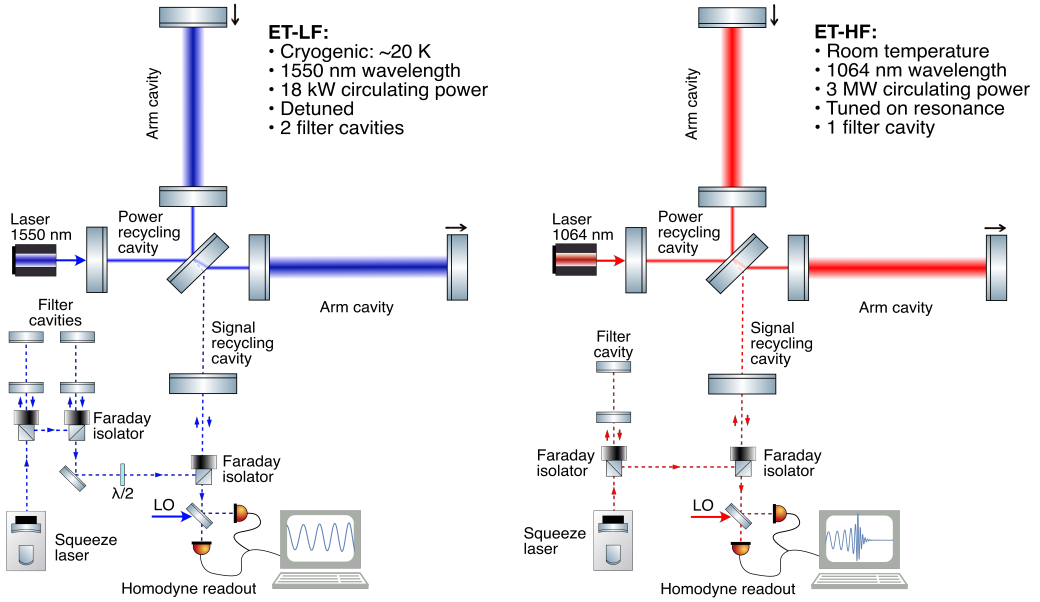

Figure 1. Schematic design of the Einstein Telescope detectors: low frequency (**left**) and high frequency (**right**). Both detectors will be co-located in the underground facility. The main parameters are listed in the inset. Signal recycling cavity (SRC) of the ET-LF is displaced to detune the detector from its resonance and create an optical spring. Squeeze laser injects quantum correlated light in the signal port of the detector, after reflecting it off the detuned filter cavities. The ET-LF features two filter cavities to operate in detuned configuration. The ET-HF uses only one. The signal together with quantum field is overlapped with a strong coherent field of a local oscillator (LO) in a homodyne readout setup. Black arrows indicate the differential changes in arm length (caused by GWs or displacement noise) leading to the appearance of the signal at the readout.

2. Quantum Noise in GW Detectors

2.1. Quantum Noise and the SQL

Modern GW detectors, i.e., Advanced LIGO, Advanced Virgo, GEO600, and KAGRA, are Michelson laser interferometers. Passing GWs shrink and stretch distances between the central beam-splitter and the end mirrors of arm cavities, which are suspended such that they move as free masses along the laser beams. The differential change in length is seen as amplitude modulation in laser power on the output field. In a simple interferometer, this amplitude modulation is too small to be detectable. Therefore, modern detectors enhance light power as well as the signal in the arms using arm cavities as well as a power recycling cavity. An additional mirror at the signal port of the interferometer forms a signal recycling cavity (SRC), which allows increasing detection bandwidth [66,67] or modifying the frequency response via the optical spring effect, as we will discuss in the next section. Future detectors, such as the ET and the CE, will also feature longer arms to further boost the sensitivity, which improves with increased arm length.

The detector is typically tuned so that, in the absence of a GW signal, all laser power is reflected back toward the laser, leaving the signal port of the interferometer dark. According to quantum mechanics, even when the average power in the field is zero, a quantum vacuum field in the ground state is still present. This vacuum field enters the signal port, propagates through the interferometer, and exits the signal port again. The ground-state uncertainty in its signal (phase) quadrature leads to SN, which manifests as power fluctuations in the DC readout [68], as used in Advanced LIGO and Advanced Virgo at the time of writing, or the homodyne readout [69,70], planned for all future detectors. As

the vacuum field propagates through the interferometer, it interacts with mirrors through radiation pressure. The uncertainty in the amplitude quadrature of the field is amplified by the coherent power in the arms, giving rise to strong QRPN. The interaction between light and mirrors generates quantum correlations between the light and the motion of the mirrors, as recently observed by Advanced LIGO [71]. These interactions correlate SN and QRPN through the ponderomotive squeezing effect [19,72–76]. However, these correlations are not typically observed directly in the signal quadrature at the detector output, unless the readout is optimized for that [20,34]. The two quadratures of the quantum vacuum field define two types of quantum noise in the detector. This quantum vacuum field state can be replaced with another quantum state specifically engineered to suppress one of the quadratures or to introduce additional correlations between SN and QRPN, as will be discussed later in the text.

Most generally, quantum-noise-limited sensitivity of the detector is described by the sum of the SN, QRPN and their cross-correlation term [20]:

$$S_h(\Omega) = \frac{8}{L^2}\left[S_{\mathrm{SN}}(\Omega) + 2\Re[\chi^*(\Omega)S_{\mathrm{CC}}(\Omega)] + |\chi(\Omega)|^2 S_{\mathrm{QRPN}}(\Omega)\right], \tag{1}$$

where $\chi(\Omega)$ is the mechanical response function of the suspended mirrors of arm cavities (including any possible modification), L is the arm length, and $S_{\mathrm{SN}}(\Omega)$, $S_{\mathrm{QRPN}}(\Omega)$, and $S_{\mathrm{CC}}(\Omega)$ are, respectively, spectral density of SN, spectral density of QRPN, and the cross-correlation spectral density of these two noises. They obey the following uncertainty relation:

$$S_{\mathrm{SN}}(\Omega)S_{\mathrm{QRPN}}(\Omega) - |S_{\mathrm{CC}}(\Omega)|^2 \geq \frac{\hbar^2}{4\eta(\Omega)}, \tag{2}$$

where $\eta \leq 1$ is the total quantum efficiency of the detector, which takes into account optical losses and quantum efficiency of photodetection.

Each quantum noise contribution scales differently with light power: SN decreases with increasing power, while QRPN increases (when normalized to the transfer function of a GW signal through the interferometer). In the absence of quantum correlations, each signal frequency has an optimal power at which these two noise sources become equal, minimizing their combined spectral density. The locus of these minimal noise points across frequencies defines the standard quantum limit (SQL). For a given light power, the detector's sensitivity touches the SQL at only one specific frequency. To show this, we can simplify Equation (1) in the absence of cross-correlation between the noises, $S_{\mathrm{CC}}(\Omega) = 0$, assuming mirrors to be free masses M with response $\chi(\Omega)^{-1} = -M\Omega^2$. In the resulting expression the SQL can be introduced explicitly [34]:

$$S_h(\Omega) = \frac{S_{\mathrm{SQL}}(\Omega)}{2}\left(\underbrace{\frac{1}{\mathcal{K}(\Omega)}}_{\mathrm{SN}} + \underbrace{\mathcal{K}(\Omega)}_{\mathrm{QRPN}}\right), \tag{3}$$

$$S_{\mathrm{SQL}}(\Omega) = \frac{8\hbar}{L^2 M\Omega^2} \tag{4}$$

where $\hbar$ is the reduced Plank constant and $\mathcal{K}(\Omega)$ is the so-called Kimble factor [34], which describes the coupling between the light and the motion of the mirror due to radiation pressure. The Kimble factor depends on the specific configuration of the detector. For a

typical cavity-enhanced Michelson interferometer operating without detuning, such as the ET-HF, this factor becomes:

$$\mathcal{K}(\Omega) = \frac{8\omega_0 P_c}{McL} \frac{\kappa}{\Omega^2(\kappa^2 + \Omega^2)}, \tag{5}$$

where κ is the detection bandwidth, c is the speed of light, P_c is the power inside the arm cavities, and ω_0 is the laser frequency. An important takeaway from this equation is that for a given power P_c, the sensitivity becomes equal to the SQL only at one frequency. It can never overcome the SQL through classical modifications, such as increasing laser power or changing the cavity parameters. Achieving sensitivity beyond the SQL requires quantum technologies. These technologies, often referred to as quantum nondemolition (QND) loosely fit into three categories: modifying the quantum state of the light, changing the response of the detector, and modifying the detection scheme [20,34,35]. The ET will employ the first two categories.

The most established and successful method for modifying the quantum state of light is quantum squeezing [21,22,77–80]. Squeezed light reduces uncertainty in one quadrature of the light field at the expense of increasing uncertainty in the other, ensuring the Heisenberg uncertainty principle remains satisfied [23,24]. Squeezed light is generated through a nonlinear optical process in which a photon from the pump field is converted into two lower-energy photons in the signal field [81,82]. These two photons exhibit strong correlations in both time and frequency. In the case of a continuous light field, these correlations manifest as two sideband fields symmetrically positioned around the central frequency. In GW detectors, a squeeze laser injects quantum correlated field into the signal port [18,23,30,80] and the resulting sensitivity introduced in Equation (3) becomes:

$$S_h(\Omega) = \frac{S_{\mathrm{SQL}}(\Omega)}{2} \left(\underbrace{\frac{1}{\beta\mathcal{K}(\Omega)}}_{\mathrm{SN}} + \underbrace{\beta\mathcal{K}(\Omega)}_{\mathrm{QRPN}} \right), \tag{6}$$

where $\beta = e^{2r}$ is the squeeze factor, with r being the squeeze parameter [83]. This expression illustrates that while SN (the first term) is suppressed by β, QRPN (the second term) is proportionally enhanced. This trade-off allows to selectively suppress or enhance SN or QRPN [84,85]. At the same time, it makes achieving high broad-band sensitivity impossible without introducing more complex quantum schemes. Additionally, the SQL still limits the best achievable sensitivity.

2.2. Overcoming the SQL

Overcoming the SQL generally requires nonzero cross-correlation between SN and QRPN, as indicated by Equation (1). For example, it is possible to surpass the SQL in a narrow frequency band by creating correlations between the amplitude and phase quadratures when injecting squeezed light along an intermediate quadrature. In 2020, Advanced LIGO used this approach to observe correlations between the light field and the motion of the mirrors of arm cavities [71,86]. To suppress quantum noise across all frequencies, the squeeze factor must become frequency-dependent: suppressing QRPN at low frequencies and transitioning to suppress SN at high frequencies; see Figure 2. Such frequency-dependent rotation can be achieved by reflecting the squeezed vacuum field off detuned single-sided cavities, which imprint a frequency-dependent phase shift onto the squeeze field (ideally) without altering its properties [34]. Development of frequency-dependent squeezing for GW detectors began in late 2000s [87–91], culminating in the deployment of the technology in Advanced LIGO in 2023 [32]. In 2024, Advanced LIGO successfully demonstrated sensi-

tivity below the SQL using this technique [92], marking a significant milestone in quantum noise suppression for GW detection.

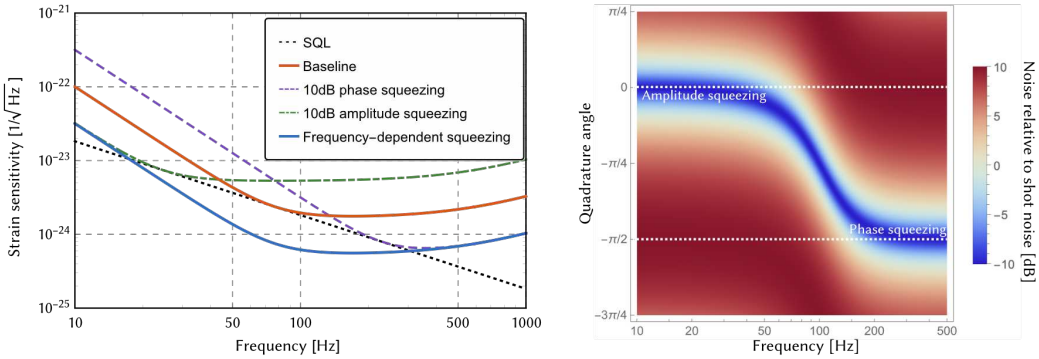

Figure 2. (**left**) Sensitivity of a GW detector enhanced with squeezed light. The baseline sensitivity without quantum enhancement is shown in solid orange. Phase squeezing (dashed violet) increases the sensitivity at high frequencies, at a price of reduced low-frequency sensitivity, which increases due to QRPN. Amplitude squeezing (dash-dotted green) allows suppressing QRPN at low frequencies, increasing the SN at high frequencies. For both phase and amplitude squeezing, sensitivity does not surpass the SQL (dotted black), since no cross-correlation between the noises is used. Frequency-dependent squeezing allows to rotate the squeezed quadratures, such that the noise is suppressed at all frequencies, allowing to surpass the SQL (solid blue). (**right**) Injected frequency-dependent squeezing as a function of the quadrature angle and frequency, showing the rotation of the squeeze quadrature from amplitude quadrature at low frequency to phase quadrature at high frequency.

The second approach to overcoming the SQL is modifying the response of the detector. The ET-LF will use the so-called optical spring effect to achieve this [66,93–99]. If a detector is detuned from its resonance condition, the field amplitude in the detector cavities becomes dependent on the position of the arm cavity mirrors (cavity length). In turn, this position is influenced by the radiation pressure force, which itself depends on the field amplitude. This feedback mechanism results in a position-dependent force, acting on the mirror, changing its dynamics similarly to a spring (or anti-spring). Notably, this effect resonantly enhances the sensitivity at the optical spring frequency, which will allow the sensitivity to surpass the SQL. The challenge of this approach is that the system becomes intrinsically unstable. Realization of the control on such systems in a large-scale detector remains an open question. Coherent stabilization approaches have been proposed [96], but their detailed realization requires further studies. To date, the optical spring approach has only been demonstrated on table-top experiments [100–106]. Interestingly, the effect can be used as a tool for high-quality laser power stabilization [107].

There are many other quantum technological approaches, such as speedmeter configurations [108–118], internal filters [119–133], and alternative detector topologies [35,134–136]. They allow suppressing quantum noise in different ways, but we limit the discussion to the two main approaches described above, as they are directly applied in the ET.

2.3. Optical Loss and Phase Noise

There are two major limitations on the application of squeezed light in the detector: optical losses and phase noise. Optical losses occur due to absorption in the mirror material, nonideal reflectivities of the mirrors, clipping of light beams on different components, scattering on imperfections, or direct contamination of mirror surfaces [137]. Each optical loss source can be modeled as a beam splitter, which not only reduces the field amplitude, but also mixes in unsqueeezed vacuum field, which further decreases the squeeze level.

The noise power spectral density of a squeezed quadrature experiencing the loss of λ is described by:

$$S = \beta^{-1}(1-\lambda) + \lambda. \tag{7}$$

The effect of the loss is quite drastic, as seen in Figure 3: for example, with 10% of loss, it is impossible to detect more than 10 dB of squeezing (which corresponds to a factor of $\approx$3 increase in detector sensitivity). Considering the large number of optical components and the overall complexity of the detector's optical layout, achieving 10% loss demands significant technological effort. In general, optical losses set the fundamental quantum limit on the achievable sensitivity of the detector [124,133,138].

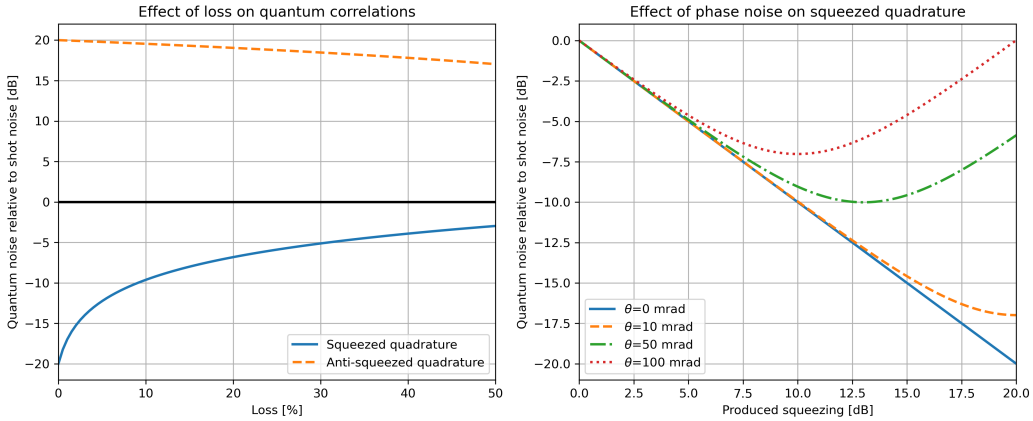

Figure 3. Effects of decoherence on squeezed light. (**Left**) Reduction of squeeze (anti-squeeze) values as a function of detection loss. At 10% loss, the initial 20 dB of squeezing is reduced below 10 dB; at 50% loss, less than 3 dB of squeezing is observed. The effect on the anti-squeezed quadrature is less pronounced. Black line at 0 dB corresponds to the case without any squeezing and serves as a reference. (**Right**) The effect of phase noise on detected squeezing as a function of produced squeezing. The higher the initial squeeze value, the greater the impact of phase noise due to the stronger coupling of the anti-squeezed quadrature.

Phase noise originates from fluctuations in the optical paths within the detector, which alter the relative phase between the squeezed field and the local oscillator in the homodyne readout. This leads to coupling of the anti-squeezed quadrature into the squeezed quadrature [139,140]:

$$S = \beta^{-1}\cos^2\theta + \beta\sin^2\theta, \tag{8}$$

where θ is the average phase angle fluctuation. Since β is typically much larger than 1, even a small phase fluctuation (on the order of a few tens of mrad) is enough to significantly impact the squeeze level; see Figure 3. Precise control of optical path lengths everywhere in the detector allows to minimize the impact of phase noise.

3. Quantum Enhancement for the Einstein Telescope

Frequency-dependent squeezing is essential for the success of the ET. However, its implementation is very different for the LF and the HF detector. The LF is detuned such that the optical spring would significantly amplify the signals in a narrow frequency band. The HF is tuned on resonance and aims to detected GWs in a broad frequency band. These regimes affect the design of frequency-dependent squeezing; see Figure 4 for a conceptual demonstration of quantum enhancement on the sensitivity.

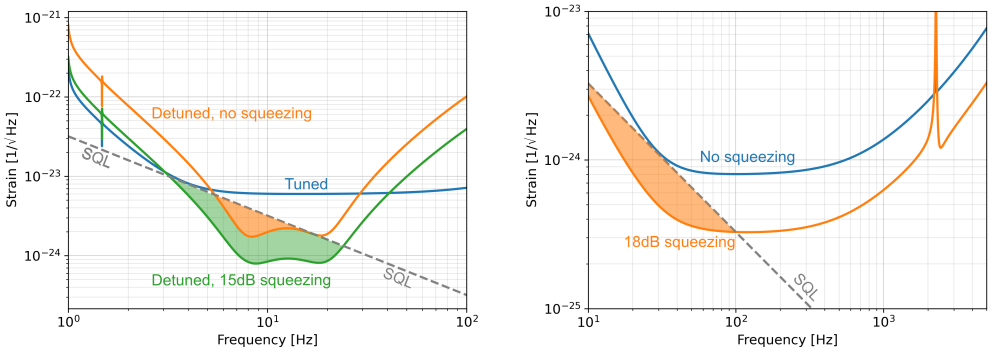

Figure 4. Frequency-dependent squeezing in the ET. (**left**) Comparison between the three configurations of the LF detector: tuned (blue), limited by the SQL (dashed gray); detuned, featuring the optical spring (orange); and enhanced by both the optical spring and the frequency-dependent squeezing (green). Both optical spring configurations allow to overcome the SQL. Shaded areas highlight sub-SQL sensitivity. (**right**) The ET-HF with (orange) and without (blue) frequency-dependent squeezing. In both plots, frequency-dependent squeezing allows to enhance the nonsqueezed sensitivity across the full detection band. Figure 5 shows the contributions of different imperfections in these curves.

In theory, achieving perfect frequency-dependent squeezing would require an infinite number of filter cavities, owing to the specific shape of their phase response. In practice, however, two filter cavities are sufficient to achieve the necessary frequency rotation [34]. Furthermore, when the detector's detection bandwidth is broad—specifically, when the bandwidth significantly exceeds the frequency where SN and QRPN are equal—a single filter cavity is sufficient. This condition is met in the case of the ET-HF. In contrast, the sensitivity of the ET-LF exhibits two distinct minima, requiring at least two filter cavities, each optimized to address a specific minimum.

Figure 5 shows quantum enhancement of the ET and specific contributions from different noise sources. We can distinguish two main contributions, as discussed above: optical loss and phase noise (or similar effects). There are several sources of optical loss:

- *Injection loss*, which occurs on the way from the squeeze laser to the interferometer, including several Faraday isolators and imperfect state generation in the squeeze laser cavity.
- *Readout loss*, which includes all optical components from the interferometer to photodetectors. Of particular note here are output mode cleaners: cavities used to separate the single optical mode carrying the signal from other parasitic and technical light fields. This also includes imperfect balancing of the homodyne readout and imperfect quantum efficiency of photodetectors.
- *SRC loss*, which occurs inside the SRC cavity, mainly due to the central beam splitter and its anti-reflective coatings.
- *Mode mismatch*, which occurs due to mismatches in the shapes of transverse optical modes between different interfaces and introduces anomalous loss.
- *Filter cavity loss*, which occurs inside the filter cavity, has a profound impact on the sensitivity, which we discuss in detail below.

3.1. Optical Loss in Filter Cavities

This impact is two-fold: (i) a part of the squeezed field is lost and replaced by a vacuum and (ii) there is a so-called dephasing mechanism caused by the unequal amount of round-trips inside the filter cavity experienced by two sidebands of the squeezed field. The second mechanism was only recently identified [141,142] and subsequently analyzed in detail through theoretical studies [143]. It was, however, quickly recognized as the primary

limiting factor for quantum noise in the ET-LF. Dephasing occurs due to different amount of loss experienced by the lower and the upper sidebands of the squeezed field, as they are reflected off a detuned cavity. For example, lower sideband might be almost fully reflected and never enters the cavity, while upper sideband is close to resonance and experiences strong loss. The resulting effect is very similar to that of a phase noise: anti-squeezing couples strongly into the squeezed quadrature.

Reducing optical losses inside the filter cavity is thus of central importance, especially for the ET-LF. A realistic design of filter cavities takes into account all possible sources of decoherence [144–146]. However, achieving the level of optical loss per mirror assumed in the ET design requires substantial technological advancements. A complementary approach to enhancing mirror quality is extending the lengths of the filter cavities. To explain this, we note that the phase rotation upon reflection off the cavity depends only on the cavity linewidth and detuning from resonance. Cavity linewidth is defined by the ratio between the losses in the cavity (including front mirror) and the cavity length L: $\gamma = c(T + \lambda)/4L$, where c is the speed of light and λ includes all losses in the cavity per one round trip except the front mirror power transmission T. The relevant value for the filter cavity is, thus, not the loss itself, but the loss per unit length [144]. A useful measure is quantum enhancement relative to the SQL, which can be approximated as [34]:

$$\sqrt{S_h / S_h^{\mathrm{SQL}}} \geq \left(\frac{\lambda c}{\beta \gamma L} \right)^{1/4}. \tag{9}$$

This equation highlights the main property: if the cavity linewidth γ and loss per round trip λ are fixed, only increasing the filter cavity length L can reduce the detrimental effect of losses on sensitivity. The effect is more relevant for the ET-LF, since its low frequency operation requires filter cavities with very narrow linewidths ($\approx$8 Hz for one of the cavities) and the impact of loss is strong. For the ET-HF, the transition between QRPN and SN is at much higher frequency, and therefore, the linewidth of the filter cavity is about 3 times larger ($\approx$22 Hz). Furthermore, frequencies at which the ET-HF is limited by QRPN mostly do not contribute to the combined sensitivity of the ET-LF and the ET-HF or are limited by other noises, such as the suspension and the coating thermal noises. This allows to relax the constraints on the filter cavity loss, reducing its length compared to the ET-LF. It is worth noting that the loss per round trip also depends on the cavity length, due to the increased beam size for longer cavities and associated scattering losses [145,147–149], which has to be accounted for in any practical design.

Dephasing has an additional indirect impact on squeezing: in the presence of loss in the filter cavity, it may be optimal to reduce the amount of anti-squeezing, such that its coupling is minimized. However, this also means a reduction in the squeeze factor at all frequencies. For instance, direct optical loss may allow observing 10 dB of squeezing, but the need to reduce anti-squeezing results in only 8 dB of detected squeezing. This balance requires careful optimization in the design process.

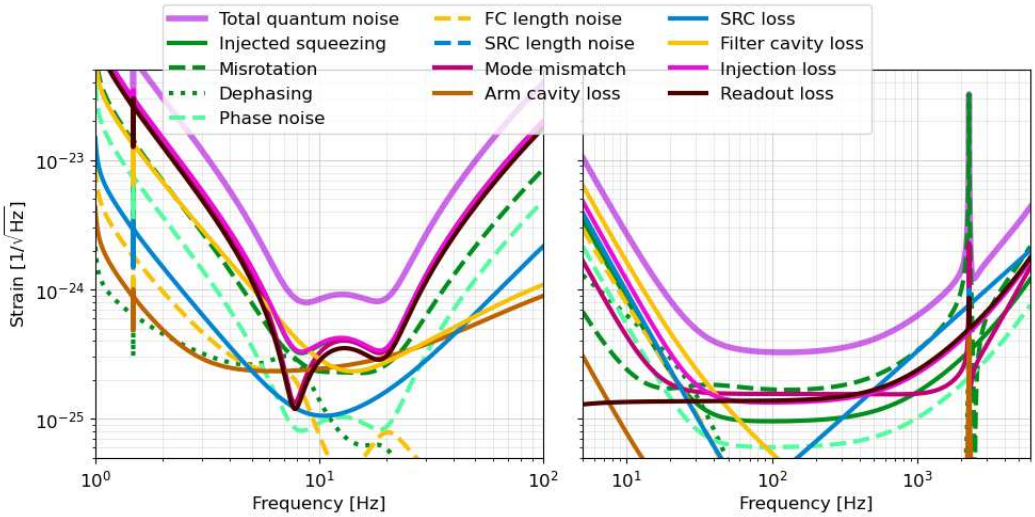

Figure 5. Example of possible decoherence contributions to quantum noise in the ET-LF (**left**) and -HF (**right**). The solid green line corresponds to sensitivity without loss contribution (for the LF in this example, it almost coincides with the curve for injection loss contribution). Other curves show contributions from different noise mechanisms, which are added as squares to produce the final violet line, representing the square root of this sum. For the LF, the main limitations are coming from filter cavity loss, injection and readout loss, and mode mismatch. For the HF, filter cavity loss is limiting at a low frequency, and SRC loss is strongly limiting at a high frequency. Of note is a feature at ∼2 kHz arising from mode mismatch. Other important contributions are misrotation of the squeezing ellipse, arising from suboptimal rotation applied by the filter cavities, and length noise in SRC and filter cavities, originating optical path fluctuations due to residual motion of the various optical components. For these plots, we consider a filter cavity length of 5 km and 15 dB of squeezing for the LF and a filter cavity length of 1 km and 18 dB of squeezing for the HF. Other parameters are generally based on the design published in Ref. [49]. Note that these curves do not represent the official ET noise budget, but are an example of the possible noise breakdown based on the pyGWINC simulation package [150].

3.2. Other Sources of Decoherence

Mode mismatch is a significant source of decoherence in GW detectors. Efficient interference between optical modes requires that their transverse shapes match perfectly. However, in practice, small mismatches are unavoidable. These can occur, e.g., between the squeezed field and the filter cavity mode, between the filter cavity and the interferometer, or even between the two interferometer arms. Mode mismatch leads to coherent effects: for instance, if the squeezed field is scattered into a higher-order spatial mode at one interface and subsequently scattered back into the fundamental mode at another interface, this can introduce significant decoherence [142]. The phases of the fundamental and higher-order modes at the second interface may differ due to propagation or coupling changes. At this point, the squeezing ellipse in the higher-order mode may become rotated relative to the fundamental mode. When the modes interact again, a substantial fraction of anti-squeezing may couple into the squeezed field, effectively degrading the squeezing [151]. This process manifests similarly to phase noise and may require a reduction in both the squeezing and anti-squeezing levels to minimize detrimental effects on the detector sensitivity. This change is frequency dependent and leads to an overall reduction in the detector performance. At present, no detailed model exists to quantify the impact of mode mismatch on quantum noise, although important steps have been made in this direction [142]. Further research is required to evaluate its effects on sensitivity and to develop strategies for mitigation. For instance, in some scenarios, mitigation of mode mismatch effects may be possible by

squeezing the higher-order modes that couple into the detector [152]. Active strategies for controlling mode shapes also need to be employed [153].

There are several contributions to the phase noise in the detector [15,140]: residual length noise of the SRC and filter cavities, as well as residual fluctuations of in-path suspended steering optics, which are generally actively suppressed, but only to a certain degree [154]. Another important contribution to the phase noise is back-scattered light, where a portion of optical power leaking from the interferometer propagates towards the squeeze laser, interacts with the squeezed field, and adds fluctuation of the squeeze phase [155]. Active strategies to control it will be implemented [155].

3.3. Alternative Configurations

Constructing long filter cavities is a significant technological and financial challenge in detector design, as it requires large-volume tunnel excavation and extensive vacuum systems. Several alternative approaches have been proposed to realize frequency-dependent squeezing without relying on long filter cavities. Among these, one of the most prominent is the so-called EPR squeezing technique [156–158]. This approach takes advantage of the long arm cavities of the detector itself, using them as substitutes for dedicated filter cavities. To achieve this, two entangled fields are generated: one tuned to the detector's resonance around the signal frequencies and the other far outside this range, near the next longitudinal resonances of the arm cavities. The second field does not interact with the GW signal but can be detuned relative to the cavity resonance to acquire the necessary frequency dependence before being independently detected. The two entangled beams are quantum-correlated, and after detection, an optimal combination of the measurement records allows the frequency dependence of the auxiliary beam to be projected onto the main beam, effectively creating frequency-dependent squeezing. This approach takes full advantage of the exceptional optical quality of the detector's mirrors and the long cavity lengths, which are intrinsic to GW observatories. However, this technique has notable downsides. First, it requires two homodyne readouts instead of one, which reduces the quantum enhancement by 3 dB. Second, the optical losses are effectively doubled, as they impact both entangled beams, further diminishing the achievable squeezing. While this technique has been successfully demonstrated in table-top experiments [159–161], its implementation in the ET requires further study. For instance, the original proposal is limited to replacing a single filter cavity and, therefore, is not directly applicable to the ET-LF, which requires two filter cavities to accommodate its dual-minima sensitivity profile. Conceptual modifications to this technique have been proposed to extend it to the ET-LF [162], but further studies, both experimental and theoretical, are needed to understand the feasibility of the approach.

Another alternative to frequency-dependent squeezing, which is in the early stages of development, is the use of effective negative mass oscillators [163,164]. Coupling spin ensemble to a GW detector allows the modification of the response of the combined system and significantly suppress QRPN. This approach has been demonstrated in table-top experiments [165,166], and theoretically studied in detail for GW detection [167,168]. It requires further detailed technical assessment to consider its feasibility as the alternative to filter cavities.

4. Discussion and Outlook

Quantum technology lies at the heart of the ET and is the key to achieving its goals. Quantum noise is the primary factor limiting the detector's sensitivity across most of its detection band. Successfully suppressing this noise is essential for realizing the full potential of the ET, a facility designed to operate at the cutting edge of science for several decades.

Modern squeeze lasers already provide high-quality squeezed states that meet many of the requirements for the ET [79,169–171]. However, delivering and maintaining a high degree of frequency-dependent squeezing inside the detector presents significant challenges. One of the most important is the need to minimize and account for all sources of optical loss. At first glance, the impact of potential added loss on the sensitivity may appear minor, as it only reduces it by a few tens of percentage points; see Figure 6 (left). However, when translated to the cosmological reach, it becomes rather significant, see Figure 6 (right). For instance, a 25% increase in noise around 8 Hz leads to a drop in redshift from 98 to 92; see Ref. [49] for an overview of the impact of sensitivity changes on the science case. Therefore, it is of utmost importance to minimize every possible loss contribution, especially in filter cavities. This could be achieved by characterizing and optimizing existing coatings [137], developing new coating solutions, increasing the filter cavity lengths, or, most likely, employing all of these approaches. Another critical aspect is the control of transverse mode shapes within the interferometer. This will necessitate precise control of mirror surface shapes, management of thermal effects that could distort the optical paths, especially in high-power the ET-HF [172,173], and maintaining optimal alignment through adaptive optics [153].

Beyond GW detection, the quantum technologies employed in the ET hold the promise of exploring new frontiers in fundamental physics. They will allow preparing and studying macroscopic quantum states of the mirrors, probing the limits of quantum mechanics, testing gravity-induced decoherence, and investigating other quantum effects [86,174]. Such capabilities position the ET as not only a GW observatory but also a platform for groundbreaking research into the foundations of quantum theory.

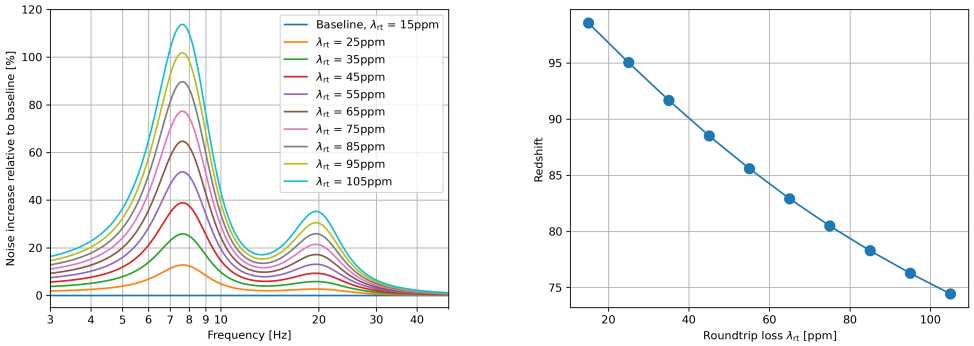

Figure 6. Effect of filter cavity loss on the quantum noise of the ET-LF (**left**) and its cosmological reach (**right**). Any small loss added to the baseline roundtrip loss of 15 ppm (15×10^{-6}) results in a noise increase, particularly around the 8 Hz optical spring resonance, primarily due to dephasing. The effect on the cosmological reach is significant: increasing the noise by a factor of 2 (i.e., by 100%) reduces the redshift from almost 100 to 76. Here, the squeeze value is not optimized for each loss value, so in practice, the impact might be reduced at the peak frequency at the price of increased noise in the broad band. The redshift here is computed as the maximal reach for equal mass nonspinning binaries by using the `inspiral_range` tool [175].

Funding: This research received no external funding.

Acknowledgments: The author thanks Julian Gurs for advice on the manuscript. This work was supported by the Deutsche Forschungsgemeinschaft (DFG) under Germany's Excellence Strategy EXC 2121 "Quantum Universe"-390833306.

Conflicts of Interest: The author declares no conflicts of interest.

References

1. Aasi, J.; Abbott, B.P.; Abbott, R.; Abbott, T.; Abernathy, M.R.; Ackley, K.; Adams, C.; Adams, T.; Addesso, P.; Adhikari, R.X.; et al. Advanced LIGO. *Class. Quantum Gravity* **2015**, *32*, 074001. [CrossRef]
2. Acernese, F.; Adams, T.; Agatsuma, K.; Aiello, L.; Allocca, A.; Amato, A.; Antier, S.; Arnaud, N.; Ascenzi, S.; Astone, P.; et al. Advanced Virgo Status. *J. Phys. Conf. Ser.* **2020**, *1342*, 012010. [CrossRef]
3. Dooley, K.L.; LIGO Scientific Collaboration. Status of GEO 600. *J. Phys. Conf. Ser.* **2015**, *610*, 012015. [CrossRef]
4. KAGRA Collaboration. KAGRA: 2.5 Generation Interferometric Gravitational Wave Detector. *Nat. Astron.* **2019**, *3*, 35–40. [CrossRef]
5. Abbott, B.P.; Abbott, R.; Abbott, T.D.; Abernathy, M.R.; Acernese, F.; Ackley, K.; Adams, C.; Adams, T.; Addesso, P.; Adhikari, R.X.; et al. Observation of Gravitational Waves from a Binary Black Hole Merger. *Phys. Rev. Lett.* **2016**, *116*, 061102. [CrossRef]
6. The LIGO Scientific Collaboration. Binary Black Hole Mergers in the First Advanced LIGO Observing Run. *Phys. Rev. X* **2016**, *6*, 041015. [CrossRef]
7. Abbott, B.P.; Abbott, R.; Abbott, T.D.; Abraham, S.; Acernese, F.; Ackley, K.; Adams, C.; Adhikari, R.X.; Adya, V.B.; Affeldt, C.; et al. GWTC-1: A Gravitational-Wave Transient Catalog of Compact Binary Mergers Observed by LIGO and Virgo during the First and Second Observing Runs. *Phys. Rev. X* **2019**, *9*, 31040. [CrossRef]
8. Abbott, R.; Abbott, T.D.; Acernese, F.; Ackley, K.; Adams, C.; Adhikari, N.; Adhikari, R.X.; Adya, V.B.; Affeldt, C.; Agarwal, D.; et al. GWTC-2.1: Deep Extended Catalog of Compact Binary Coalescences Observed by LIGO and Virgo during the First Half of the Third Observing Run. *Phys. Rev. D* **2024**, *109*, 022001. [CrossRef]
9. Abbott, R.; Abbott, T.D.; Acernese, F.; Ackley, K.; Adams, C.; Adhikari, N.; Adhikari, R.X.; Adya, V.B.; Affeldt, C.; Agarwal, D.; et al. GWTC-3: Compact Binary Coalescences Observed by LIGO and Virgo during the Second Part of the Third Observing Run. *Phys. Rev. X* **2023**, *13*, 041039. [CrossRef]
10. The LIGO Scientific Collaboration. Multi-Messenger Observations of a Binary Neutron Star Merger. *Astrophys. J. Lett.* **2017**, *848*. [CrossRef]
11. Abbott, B.P.; Abbott, R.; Abbott, T.D.; Acernese, F.; Ackley, K.; Adams, C.; Adams, T.; Addesso, P.; Adhikari, R.X.; Adya, V.B.; et al. Gravitational Waves and Gamma-Rays from a Binary Neutron Star Merger: GW170817 and GRB 170817A. *Astrophys. J.* **2017**, *848*, L13. [CrossRef]
12. The LIGO Scientific Collaboration and The Virgo Collaboration; Abbott, B.P.; Abbott, R.; Abbott, T.D.; Acernese, F.; Ackley, K.; Adams, C.; Adams, T.; Addesso, P.; Adhikari, R.X.; et al. A Gravitational-Wave Standard Siren Measurement of the Hubble Constant. *Nature* **2017**, *551*, 85–88. [CrossRef]
13. Abbott, B.P.; Abbott, R.; Abbott, T.D.; Abernathy, M.R.; Ackley, K.; Adams, C.; Addesso, P.; Adhikari, R.X.; Adya, V.B.; Affeldt, C.; et al. Exploring the Sensitivity of next Generation Gravitational Wave Detectors. *Class. Quantum Gravity* **2017**, *34*, 044001. [CrossRef]
14. Martynov, D.V.; Hall, E.D.; Abbott, B.P.; Abbott, R.; Abbott, T.D.; Adams, C.; Adhikari, R.X.; Anderson, R.A.; Anderson, S.B.; Arai, K.; et al. Sensitivity of the Advanced LIGO Detectors at the Beginning of Gravitational Wave Astronomy. *Phys. Rev. D* **2016**, *93*, 112004. [CrossRef]
15. Tse, M.; Yu, H.; Kijbunchoo, N.; Fernandez-Galiana, A.; Dupej, P.; Barsotti, L.; Blair, C.D.; Brown, D.D.; Dwyer, S.E.; Effler, A.; et al. Quantum-Enhanced Advanced LIGO Detectors in the Era of Gravitational-Wave Astronomy. *Phys. Rev. Lett.* **2019**, *123*, 231107. [CrossRef]
16. Acernese, F.; Agathos, M.; Aiello, L.; Allocca, A.; Amato, A.; Ansoldi, S.; Antier, S.; Arène, M.; Arnaud, N.; Ascenzi, S.; et al. Increasing the Astrophysical Reach of the Advanced Virgo Detector via the Application of Squeezed Vacuum States of Light. *Phys. Rev. Lett.* **2019**, *123*, 231108. [CrossRef]
17. Buikema, A.; Cahillane, C.; Mansell, G.L.; Blair, C.D.; Abbott, R.; Adams, C.; Adhikari, R.X.; Ananyeva, A.; Appert, S.; Arai, K.; et al. Sensitivity and Performance of the Advanced LIGO Detectors in the Third Observing Run. *Phys. Rev. D* **2020**, *102*, 062003. [CrossRef]
18. Caves, C. Quantum-Mechanical Noise in an Interferometer. *Phys. Rev. D* **1981**, *23*, 1693–1708. [CrossRef]
19. Braginsky, V.B.; Manukin, A.B. Ponderomotive Effects of Electromagnetic Radiation. *Sov. Phys. JETP* **1967**, *25*, 653–655.
20. Danilishin, S.L.; Khalili, F.Y. Quantum Measurement Theory in Gravitational-Wave Detectors. *Living Rev. Relativ.* **2012**, *15*, 5. [CrossRef] [PubMed]
21. Walls, D.F. Squeezed States of Light. *Nature* **1983**, *306*, 141–146. [CrossRef]
22. Yuen, H. Two-Photon Coherent States of the Radiation Field. *Phys. Rev. A* **1976**, *13*, 2226–2243. [CrossRef]
23. Schnabel, R. Squeezed States of Light and Their Applications in Laser Interferometers. *Phys. Rep.* **2017**, *684*, 1–51. [CrossRef]
24. Schnabel, R. 'Quantum Weirdness' in Exploitation by the International Gravitational-Wave Observatory Network. *Ann. Der Phys.* **2020**, *532*, 1900508. [CrossRef]
25. Dwyer, S.E.; Mansell, G.L.; McCuller, L. Squeezing in Gravitational Wave Detectors. *Galaxies* **2022**, *10*, 46. [CrossRef]

26. Schnabel, R.; Mavalvala, N.; McClelland, D.E.; Lam, P.K. Quantum Metrology for Gravitational Wave Astronomy. *Nat. Commun.* **2010**, *1*, 121. [CrossRef]
27. Vahlbruch, H.; Khalaidovski, A.; Lastzka, N.; Gräf, C.; Danzmann, K.; Schnabel, R. The GEO 600 Squeezed Light Source. *Class. Quantum Gravity* **2010**, *27*, 084027. [CrossRef]
28. The LIGO Scientific Collaboration. A Gravitational Wave Observatory Operating beyond the Quantum Shot-Noise Limit. *Nat. Phys.* **2011**, *7*, 962–965. [CrossRef]
29. Grote, H.; Danzmann, K.; Dooley, K.L.; Schnabel, R.; Slutsky, J.; Vahlbruch, H. First Long-Term Application of Squeezed States of Light in a Gravitational-Wave Observatory. *Phys. Rev. Lett.* **2013**, *110*, 181101. [CrossRef]
30. Barsotti, L.; Harms, J.; Schnabel, R. Squeezed Vacuum States of Light for Gravitational Wave Detectors. *Rep. Prog. Phys.* **2019**, *82*, 016905. [CrossRef] [PubMed]
31. Lough, J.; Schreiber, E.; Bergamin, F.; Grote, H.; Mehmet, M.; Vahlbruch, H.; Affeldt, C.; Brinkmann, M.; Bisht, A.; Kringel, V.; et al. First Demonstration of 6 dB Quantum Noise Reduction in a Kilometer Scale Gravitational Wave Observatory. *Phys. Rev. Lett.* **2021**, *126*, 041102. [CrossRef]
32. Ganapathy, D.; Jia, W.; Nakano, M.; Xu, V.; Aritomi, N.; Cullen, T.; Kijbunchoo, N.; Dwyer, S.E.; Mullavey, A.; McCuller, L.; et al. Broadband Quantum Enhancement of the LIGO Detectors with Frequency-Dependent Squeezing. *Phys. Rev. X* **2023**, *13*, 041021. [CrossRef]
33. Capote, E.; Jia, W.; Aritomi, N.; Nakano, M.; Xu, V.; Abbott, R.; Abouelfettouh, I.; Adhikari, R.X.; Ananyeva, A.; Appert, S.; et al. Advanced LIGO Detector Performance in the Fourth Observing Run. *arXiv* **2024**, arXiv:2411.14607. [CrossRef]
34. Kimble, H.J.; Levin, Y.; Matsko, A.B.; Thorne, K.S.; Vyatchanin, S.P. Conversion of Conventional Gravitational-Wave Interferometers into Quantum Nondemolition Interferometers by Modifying Their Input and/or Output Optics. *Phys. Rev. D* **2001**, *65*, 022002. [CrossRef]
35. Danilishin, S.L.; Khalili, F.Y.; Miao, H. Advanced Quantum Techniques for Future Gravitational-Wave Detectors. *Living Rev. Relativ.* **2019**, *22*, 2. [CrossRef]
36. Maggiore, M.; van den Broeck, C.; Bartolo, N.; Belgacem, E.; Bertacca, D.; Bizouard, M.A.; Branchesi, M.; Clesse, S.; Foffa, S.; García-Bellido, J.; et al. Science case for the Einstein Telescope. *J. Cosmol. Astropart. Phys.* **2020**, *2020*, 050. [CrossRef]
37. Punturo, M.; Abernathy, M.; Acernese, F.; Allen, B.; Andersson, N.; Arun, K.; Barone, F.; Barr, B.; Barsuglia, M.; Beker, M.; et al. The Einstein Telescope: A Third-Generation Gravitational Wave Observatory. *Class. Quantum Gravity* **2010**, *27*, 194002. [CrossRef]
38. Reitze, D.; Adhikari, R.X.; Ballmer, S.; Barish, B.; Barsotti, L.; Billingsley, G.; Brown, D.A.; Chen, Y.; Coyne, D.; Eisenstein, R.; et al. Cosmic Explorer: The U.S. Contribution to Gravitational-Wave Astronomy beyond LIGO. *arXiv* **2019**, arXiv:1907.04833. [CrossRef]
39. Evans, M.; Corsi, A.; Afle, C.; Ananyeva, A.; Arun, K.G.; Ballmer, S.; Bandopadhyay, A.; Barsotti, L.; Baryakhtar, M.; Berger, E.; et al. Cosmic Explorer: A Submission to the NSF MPSAC ngGW Subcommittee. *arXiv* **2023**, arXiv:2306.13745. [CrossRef]
40. Hall, E.D. Cosmic Explorer: A Next-Generation Ground-Based Gravitational-Wave Observatory. *Galaxies* **2022**, *10*, 90. [CrossRef]
41. Hall, E.D.; Kuns, K.; Smith, J.R.; Bai, Y.; Wipf, C.; Biscans, S.; Adhikari, R.X.; Arai, K.; Ballmer, S.; Barsotti, L.; et al. Gravitational-Wave Physics with Cosmic Explorer: Limits to Low-Frequency Sensitivity. *Phys. Rev. D* **2021**, *103*, 122004. [CrossRef]
42. Domènech, G.; Sasaki, M. Probing Primordial Black Hole Scenarios with Terrestrial Gravitational Wave Detectors. *Class. Quantum Gravity* **2024**, *41*, 143001. [CrossRef]
43. Renzini, A.I.; Goncharov, B.; Jenkins, A.C.; Meyers, P.M. Stochastic Gravitational-Wave Backgrounds: Current Detection Efforts and Future Prospects. *Galaxies* **2022**, *10*, 34. [CrossRef]
44. Sathyaprakash, B.S.; Schutz, B.F.; Van Den Broeck, C. Cosmography with the Einstein Telescope. *Class. Quantum Gravity* **2010**, *27*, 215006. [CrossRef]
45. Vitale, S.; Evans, M. Parameter Estimation for Binary Black Holes with Networks of Third-Generation Gravitational-Wave Detectors. *Phys. Rev. D* **2017**, *95*, 064052. [CrossRef]
46. Mills, C.; Tiwari, V.; Fairhurst, S. Localization of Binary Neutron Star Mergers with Second and Third Generation Gravitational-Wave Detectors. *Phys. Rev. D* **2018**, *97*, 104064. [CrossRef]
47. Ng, K.K.Y.; Isi, M.; Haster, C.J.; Vitale, S. Multiband Gravitational-Wave Searches for Ultralight Bosons. *Phys. Rev. D* **2020**, *102*, 083020. [CrossRef]
48. Ng, K.K.Y.; Vitale, S.; Farr, W.M.; Rodriguez, C.L. Probing Multiple Populations of Compact Binaries with Third-generation Gravitational-wave Detectors. *Astrophys. J. Lett.* **2021**, *913*, L5. [CrossRef]
49. Branchesi, M.; Maggiore, M.; Alonso, D.; Badger, C.; Banerjee, B.; Beirnaert, F.; Belgacem, E.; Bhagwat, S.; Boileau, G.; Borhanian, S.; et al. Science with the Einstein Telescope: A Comparison of Different Designs. *J. Cosmol. Astropart. Phys.* **2023**, *2023*, 068. [CrossRef]
50. Hild, S.; Abernathy, M.; Acernese, F.; Amaro-Seoane, P.; Andersson, N.; Arun, K.; Barone, F.; Barr, B.; Barsuglia, M.; Beker, M.; et al. Sensitivity Studies for Third-Generation Gravitational Wave Observatories. *Class. Quantum Gravity* **2011**, *28*, 094013. [CrossRef]

51. Beker, M.G.; Brand, J.F.J.V.D.; Rabeling, D.S. Subterranean Ground Motion Studies for the Einstein Telescope. *Class. Quantum Gravity* **2015**, *32*, 025002. [CrossRef]
52. Harms, J.; Naticchioni, L.; Calloni, E.; De Rosa, R.; Ricci, F.; D'Urso, D. A Lower Limit for Newtonian-noise Models of the Einstein Telescope. *Eur. Phys. J. Plus* **2022**, *137*, 687. [CrossRef]
53. Janssens, K.; Boileau, G.; Christensen, N.; Badaracco, F.; Van Remortel, N. Impact of Correlated Seismic and Correlated Newtonian Noise on the Einstein Telescope. *Phys. Rev. D* **2022**, *106*, 042008. [CrossRef]
54. Hild, S.; Chelkowski, S.; Freise, A.; Franc, J.; Morgado, N.; Flaminio, R.; DeSalvo, R. A Xylophone Configuration for a Third-Generation Gravitational Wave Detector. *Class. Quantum Gravity* **2010**, *27*, 015003. [CrossRef]
55. Nawrodt, R.; Rowan, S.; Hough, J.; Punturo, M.; Ricci, F.; Vinet, J.Y. Challenges in Thermal Noise for 3rd Generation of Gravitational Wave Detectors. *Gen. Relativ. Gravit.* **2011**, *43*, 593–622. [CrossRef]
56. Puppo, P.; Ricci, F. Cryogenics and Einstein Telescope. *Gen. Relativ. Gravit.* **2011**, *43*, 657–669. [CrossRef]
57. Koroveshi, X.; Busch, L.; Majorana, E.; Puppo, P.; Rapagnani, P.; Ricci, F.; Ruggi, P.; Grohmann, S. Cryogenic Payloads for the Einstein Telescope: Baseline Design with Heat Extraction, Suspension Thermal Noise Modeling, and Sensitivity Analyses. *Phys. Rev. D* **2023**, *108*, 123009. [CrossRef]
58. Steinlechner, J.; Martin, I.W.; Hough, J.; Krüger, C.; Rowan, S.; Schnabel, R. Thermal Noise Reduction and Absorption Optimization via Multimaterial Coatings. *Phys. Rev. D* **2015**, *91*, 042001. [CrossRef]
59. Craig, K.; Steinlechner, J.; Murray, P.G.; Bell, A.S.; Birney, R.; Haughian, K.; Hough, J.; MacLaren, I.; Penn, S.; Reid, S.; et al. Mirror Coating Solution for the Cryogenic Einstein Telescope. *Phys. Rev. Lett.* **2019**, *122*, 231102. [CrossRef]
60. Singh, N.; Bulik, T.; Belczynski, K.; Askar, A. Exploring Compact Binary Populations with the *Einstein* Telescope. *Astron. Astrophys.* **2022**, *667*, A2. [CrossRef]
61. Miller, A.L.; Singh, N.; Palomba, C. Enabling Multimessenger Astronomy with Continuous Gravitational Waves: Early Warning and Sky Localization of Binary Neutron Stars in the Einstein Telescope. *Phys. Rev. D* **2024**, *109*, 043021. [CrossRef]
62. Franciolini, G.; Iacovelli, F.; Mancarella, M.; Maggiore, M.; Pani, P.; Riotto, A. Searching for Primordial Black Holes with the Einstein Telescope: Impact of Design and Systematics. *Phys. Rev. D* **2023**, *108*, 043506. [CrossRef]
63. Iacovelli, F.; Mancarella, M.; Mondal, C.; Puecher, A.; Dietrich, T.; Gulminelli, F.; Maggiore, M.; Oertel, M. Nuclear Physics Constraints from Binary Neutron Star Mergers in the Einstein Telescope Era. *Phys. Rev. D* **2023**, *108*, 122006. [CrossRef]
64. Ota, I.; Chirenti, C. Black Hole Spectroscopy Horizons for Current and Future Gravitational Wave Detectors. *Phys. Rev. D* **2022**, *105*, 044015. [CrossRef]
65. Forteza, X.J.; Bhagwat, S.; Kumar, S.; Pani, P. Novel Ringdown Amplitude-Phase Consistency Test. *Phys. Rev. Lett.* **2023**, *130*, 021001. [CrossRef] [PubMed]
66. Buonanno, A.; Chen, Y.; Mavalvala, N. Signal Recycled Laser-Interferometer Gravitational-Wave Detectors as Optical Springs. *Phys. Rev. D* **2002**, *64*, 42001. [CrossRef]
67. Meers, B.J. Recycling in Laser-Interferometric Gravitational-Wave Detectors. *Phys. Rev. D* **1988**, *38*, 2317. [CrossRef] [PubMed]
68. Hild, S.; Grote, H.; Degallaix, J.; Chelkowski, S.; Danzmann, K.; Freise, A.; Hewitson, M.; Hough, J.; Lück, H.; Prijatelj, M.; et al. DC-readout of a Signal-Recycled Gravitational Wave Detector. *Class. Quantum Gravity* **2009**, *26*, 055012. [CrossRef]
69. Fritschel, P.; Evans, M.; Frolov, V. Balanced Homodyne Readout for Quantum Limited Gravitational Wave Detectors. *Opt. Express* **2014**, *22*, 4224. [CrossRef]
70. Steinlechner, S.; Barr, B.W.; Bell, A.S.; Danilishin, S.L.; Gläfke, A.; Gräf, C.; Hennig, J.S.; Houston, E.A.; Huttner, S.H.; Leavey, S.S.; et al. Local-Oscillator Noise Coupling in Balanced Homodyne Readout for Advanced Gravitational Wave Detectors. *Phys. Rev. D* **2015**, *92*, 072009. [CrossRef]
71. Yu, H.; McCuller, L.; Tse, M.; Kijbunchoo, N.; Barsotti, L.; Mavalvala, N.; Betzwieser, J.; Blair, C.D.; Dwyer, S.E.; Effler, A.; et al. Quantum Correlations between Light and the Kilogram-Mass Mirrors of LIGO. *Nature* **2020**, *583*, 43–47. [CrossRef] [PubMed]
72. Caves, C.M. Quantum-Mechanical Radiation-Pressure Fluctuations in an Interferometer. *Phys. Rev. Lett.* **1980**, *45*, 75–79. [CrossRef]
73. Braginsky, V.B.; Khalili, F.Y. Low Noise Rigidity in Quantum Measurements. *Phys. Lett. A* **1999**, *257*, 241. [CrossRef]
74. Braginsky, V.B.; Khalili, F.Y. *Quantum Measurement*; Cambridge University Press: Cambridge, UK, 1995.
75. Sudhir, V.; Schilling, R.; Fedorov, S.A.; Schütz, H.; Wilson, D.J.; Kippenberg, T.J. Quantum Correlations of Light from a Room-Temperature Mechanical Oscillator. *Phys. Rev. X* **2017**, *7*, 031055. [CrossRef]
76. Aggarwal, N.; Cullen, T.J.; Cripe, J.; Cole, G.D.; Lanza, R.; Libson, A.; Follman, D.; Heu, P.; Corbitt, T.; Mavalvala, N. Room-Temperature Optomechanical Squeezing. *Nat. Phys.* **2020**, *16*, 784–788. [CrossRef]
77. Vahlbruch, H.; Mehmet, M.; Chelkowski, S.; Hage, B.; Franzen, A.; Lastzka, N.; Goßler, S.; Danzmann, K.; Schnabel, R. Observation of Squeezed Light with 10-dB Quantum-Noise Reduction. *Phys. Rev. Lett.* **2008**, *100*, 033602. [CrossRef] [PubMed]
78. Mehmet, M.; Ast, S.; Eberle, T.; Steinlechner, S.; Vahlbruch, H.; Schnabel, R. Squeezed Light at 1550 Nm with a Quantum Noise Reduction of 12.3 dB. *Opt. Express* **2011**, *19*, 25763. [CrossRef] [PubMed]

79. Vahlbruch, H.; Mehmet, M.; Danzmann, K.; Schnabel, R. Detection of 15 dB Squeezed States of Light and Their Application for the Absolute Calibration of Photoelectric Quantum Efficiency. *Phys. Rev. Lett.* **2016**, *117*, 110801. [CrossRef] [PubMed]
80. Schnabel, R.; Schönbeck, A. The "Squeeze Laser". *IEEE Trans. Quantum Eng.* **2022**, *3*, 1–9. [CrossRef]
81. Collett, M.J.; Gardiner, C.W. Squeezing of Intracavity and Traveling-Wave Light Fields Produced in Parametric Amplification. *Phys. Rev. A* **1984**, *30*, 1386–1391. [CrossRef]
82. Milburn, G.; Walls, D. Production of Squeezed States in a Degenerate Parametric Amplifier. *Opt. Commun.* **1981**, *39*, 401–404. [CrossRef]
83. Stoler, D. Equivalence Classes of Minimum Uncertainty Packets. *Phys. Rev. D* **1970**, *1*, 3217–3219. [CrossRef]
84. Yap, M.J.; Cripe, J.; Mansell, G.L.; McRae, T.G.; Ward, R.L.; Slagmolen, B.J.J.; Heu, P.; Follman, D.; Cole, G.D.; Corbitt, T.; et al. Broadband Reduction of Quantum Radiation Pressure Noise via Squeezed Light Injection. *Nat. Photonics* **2020**, *14*, 19–23. [CrossRef]
85. Acernese, F.; Agathos, M.; Aiello, L.; Ain, A.; Allocca, A.; Amato, A.; Ansoldi, S.; Antier, S.; Arène, M.; Arnaud, N.; et al. Quantum Backaction on Kg-Scale Mirrors: Observation of Radiation Pressure Noise in the Advanced Virgo Detector. *Phys. Rev. Lett.* **2020**, *125*, 131101. [CrossRef] [PubMed]
86. Schnabel, R.; Korobko, M. Macroscopic Quantum Mechanics in Gravitational-Wave Observatories and Beyond. *AVS Quantum Sci.* **2022**, *4*, 014701. [CrossRef]
87. Chelkowski, S.; Vahlbruch, H.; Hage, B.; Franzen, A.; Lastzka, N.; Danzmann, K.; Schnabel, R. Experimental Characterization of Frequency Dependent Squeezed Light. *Phys. Rev.-At. Mol. Opt. Phys.* **2007**, *71*, 013806. [CrossRef]
88. Oelker, E.; Isogai, T.; Miller, J.; Tse, M.; Barsotti, L.; Mavalvala, N.; Evans, M. Audio-Band Frequency-Dependent Squeezing for Gravitational-Wave Detectors. *Phys. Rev. Lett.* **2016**, *116*, 041102. [CrossRef]
89. McCuller, L.; Whittle, C.; Ganapathy, D.; Komori, K.; Tse, M.; Fernandez-Galiana, A.; Barsotti, L.; Fritschel, P.; MacInnis, M.; Matichard, F.; et al. Frequency-Dependent Squeezing for Advanced LIGO. *Phys. Rev. Lett.* **2020**, *124*, 171102. [CrossRef] [PubMed]
90. Zhao, Y.; Aritomi, N.; Capocasa, E.; Leonardi, M.; Eisenmann, M.; Guo, Y.; Polini, E.; Tomura, A.; Arai, K.; Aso, Y.; et al. Frequency-Dependent Squeezed Vacuum Source for Broadband Quantum Noise Reduction in Advanced Gravitational-Wave Detectors. *Phys. Rev. Lett.* **2020**, *124*, 171101. [CrossRef] [PubMed]
91. Acernese, F.; Agathos, M.; Ain, A.; Albanesi, S.; Alléné, C.; Allocca, A.; Amato, A.; Amra, C.; Andia, M.; Andrade, T.; et al. Frequency-Dependent Squeezed Vacuum Source for the Advanced Virgo Gravitational-Wave Detector. *Phys. Rev. Lett.* **2023**, *131*, 041403. [CrossRef]
92. Jia, W.; Xu, V.; Kuns, K.; Nakano, M.; Barsotti, L.; Evans, M.; Mavalvala, N.; members of the LIGO Scientific Collaboration; Abbott, R.; Abouelfettouh, I.; et al. Squeezing the Quantum Noise of a Gravitational-Wave Detector below the Standard Quantum Limit. *Science* **2024**, *385*, 1318–1321. [CrossRef] [PubMed]
93. Braginsky, V.B.; Gorodetsky, M.L.; Khalili, F.Y. Optical Bars in Gravitational Wave Antennas. *Phys. Lett. A* **1997**, *232*, 340–348. [CrossRef]
94. Buonanno, A.; Chen, Y. Laser-Interferometer Gravitational-Wave Optical-Spring Detectors. *Class. Quantum Gravity* **2002**, *19*, 1569. [CrossRef]
95. Harms, J.; Chen, Y.; Chelkowski, S. Squeezed-Input, Optical-Spring, Signal-Recycled Gravitational-Wave Detectors. *Phys. Rev. D* **2003**, *68*, 042001. [CrossRef]
96. Rehbein, H.; Mueller-Ebhardt, H.; Somiya, K.; Danilishin, S.L.; Schnabel, R.; Danzmann, K.; Chen, Y. Double Optical Spring Enhancement for Gravitational Wave Detectors. *Phys. Rev. D* **2008**, *78*, 062003. [CrossRef]
97. Khalili, F.Y.; Danilishin, S.L.; Müller-Ebhardt, H.; Miao, H.; Chen, Y.; Zhao, C. Negative Optical Inertia for Enhancing the Sensitivity of Future Gravitational-Wave Detectors. *Phys. Rev.-Part. Fields Gravit. Cosmol.* **2011**, *83*, 062003. [CrossRef]
98. Korth, W.Z.; Miao, H.; Corbitt, T.; Cole, G.D.; Chen, Y.; Adhikari, R.X. Suppression of Quantum-Radiation-Pressure Noise in an Optical Spring. *Phys. Rev. A* **2013**, *88*, 33805. [CrossRef]
99. Aronson, S.; Pagano, R.; Cullen, T.; Cole, G.D.; Corbitt, T. Optical Spring Tracking for Enhancing Quantum-Limited Interferometers. *Opt. Lett.* **2024**, *49*, 6980. [CrossRef]
100. Mow-Lowry, C.M.; Mullawey, A.J.; Gossler, S.; Gray, M.B.; McClelland, D.E. Cooling of a Gramm-Scale Cantilever Flexure to 70 mK with a Servo-Modified Optical Spring. *Phys. Rev. Lett.* **2008**, *100*, 10801–10804. [CrossRef] [PubMed]
101. Cripe, J.; Danz, B.; Lane, B.; Lorio, M.C.; Falcone, J.; Cole, G.D.; Corbitt, T. Observation of an Optical Spring with a Beam Splitter. *Opt. Lett.* **2018**, *43*, 2193. [CrossRef]
102. Edgar, M.P.; Macarthur, J.; Barr, B.W.; Hild, S.; Huttner, S.; Sorazu, B.; Strain, K.A. Demonstration of an Optical Spring in the 100 g Mirror Regime. *Class. Quantum Gravity* **2016**, *33*, 075007. [CrossRef]
103. Gordon, N.A.; Barr, B.W.; Bell, A.; Graef, C.; Hild, S.; Huttner, S.H.; Leavey, S.S.; Macarthur, J.; Sorazu, B.; Wright, J.; et al. Experimental Demonstration of Coupled Optical Springs. *Class. Quantum Gravity* **2017**, *34*, 035020. [CrossRef]

104. Hossein-Zadeh, M.; Vahala, K.J. Observation of Optical Spring Effect in a Microtoroidal Optomechanical Resonator. *Opt. Lett.* **2007**, *32*, 1611. [CrossRef]
105. Sawadsky, A.; Kaufer, H.; Nia, R.M.; Tarabrin, S.P.; Khalili, F.Y.; Hammerer, K.; Schnabel, R. Observation of Generalized Optomechanical Coupling and Cooling on Cavity Resonance. *Phys. Rev. Lett.* **2015**, *114*, 043601. [CrossRef]
106. Sheard, B.S.; Gray, M.B.; Mow-Lowry, C.M.; McClelland, D.E.; Whitcomb, S.E. Observation and Characterization of an Optical Spring. *Phys. Rev. A* **2004**, *69*, 51801. [CrossRef]
107. Cullen, T.; Aronson, S.; Pagano, R.; Trad Nery, M.; Cain, H.; Cripe, J.; Cole, G.D.; Sharifi, S.; Aggarwal, N.; Willke, B.; et al. Passive Laser Power Stabilization via an Optical Spring. *Opt. Lett.* **2022**, *47*, 2746. [CrossRef]
108. Khalili, F.Y. Quantum Speedmeter and Laser Interferometric Gravitational-Wave Antennae. *arXiv* **2002**, arXiv:gr-gc/0211088. [CrossRef]
109. Danilishin, S.L. Sensitivity Limitations in Optical Speed Meter Topology of Gravitational-Wave Antennae. *Phys. Rev. D* **2004**, *69*, 102003. [CrossRef]
110. Khalili, F.Y.; Levin, Y. Speed Meter as a Quantum Nondemolition Measuring Device for Force. *Phys. Rev. D* **1996**, *54*, 4735–4737. [CrossRef] [PubMed]
111. Gräf, C.; Barr, B.W.; Bell, A.S.; Campbell, F.; Cumming, A.V.; Danilishin, S.L.; Gordon, N.A.; Hammond, G.D.; Hennig, J.; Houston, E.A.; et al. Design of a Speed Meter Interferometer Proof-of-Principle Experiment. *Class. Quantum Grav.* **2014**, *31*, 215009. [CrossRef]
112. Braginsky, V.; Khalili, F.Y. Gravitational Wave Antenna with QND Speed Meter. *Phys. Lett. A* **1990**, *147*, 251–256. [CrossRef]
113. Purdue, P. An Analisys of a QND Speed-Meter Interferometer. *Phys. Rev. D* **2002**, *66*, 22001. [CrossRef]
114. Chen, Y. Sagnac Interferometer as a Speed-Meter-Type, Quantum-Nondemolition Gravitational-Wave Detector. *Phys. Rev. D* **2003**, *67*, 122004. [CrossRef]
115. Danilishin, S.L.; Gräf, C.; Leavey, S.S.; Hennig, J.; Houston, E.A.; Pascucci, D.; Steinlechner, S.; Wright, J.; Hild, S. Quantum Noise of Non-Ideal Sagnac Speed Meter Interferometer with Asymmetries. *New J. Phys.* **2015**, *17*, 43031. [CrossRef]
116. Huttner, S.H.; Danilishin, S.L.; Barr, B.W.; Bell, A.S.; Gräf, C.; Hennig, J.S.; Hild, S.; Houston, E.A.; Leavey, S.S.; Pascucci, D.; et al. Candidates for a Possible Third-Generation Gravitational Wave Detector: Comparison of Ring-Sagnac and Sloshing-Sagnac Speedmeter Interferometers. *Class. Quantum Gravity* **2017**, *34*, 024001. [CrossRef]
117. Danilishin, S.L.; Knyazev, E.; Voronchev, N.V.; Khalili, F.Y.; Gräf, C.; Steinlechner, S.; Hennig, J.S.; Hild, S. A New Quantum Speed-Meter Interferometer: Measuring Speed to Search for Intermediate Mass Black Holes Article. *Light. Sci. Appl.* **2018**, *7*, 11. [CrossRef] [PubMed]
118. Korobko, M. Taming the Quantum Noise: How Quantum Metrology Can Expand the Reach of Gravitational-Wave Observatories. Ph.D. Thesis, University of Hamburg, Hamburg, Germany, 2020.
119. Miao, H.; Ma, Y.; Zhao, C.; Chen, Y. Enhancing the Bandwidth of Gravitational-Wave Detectors with Unstable Optomechanical Filters. *Phys. Rev. Lett.* **2015**, *115*, 211104. [CrossRef] [PubMed]
120. Somiya, K.; Kataoka, Y.; Kato, J.; Saito, N.; Yano, K. Parametric Signal Amplification to Create a Stiff Optical Bar. *Phys. Lett. A* **2016**, *380*, 521–524. [CrossRef]
121. Korobko, M.; Kleybolte, L.; Ast, S.; Miao, H.; Chen, Y.; Schnabel, R. Beating the Standard Sensitivity-Bandwidth Limit of Cavity-Enhanced Interferometers with Internal Squeezed-Light Generation. *Phys. Rev. Lett.* **2017**, *118*, 143601. [CrossRef] [PubMed]
122. Miao, H.; Yang, H.; Martynov, D. Towards the Design of Gravitational-Wave Detectors for Probing Neutron-Star Physics. *Phys. Rev. D* **2018**, *98*, 044044. [CrossRef]
123. Korobko, M.; Khalili, F.Ya.; Schnabel, R. Engineering the Optical Spring via Intra-Cavity Optical-Parametric Amplification. *Phys. Lett. A* **2018**, *382*, 2238–2244. [CrossRef]
124. Miao, H.; Smith, N.D.; Evans, M. Quantum Limit for Laser Interferometric Gravitational-Wave Detectors from Optical Dissipation. *Phys. Rev. X* **2019**, *9*, 011053. [CrossRef]
125. Bentley, J.; Jones, P.; Martynov, D.; Freise, A.; Miao, H. Converting the Signal-Recycling Cavity into an Unstable Optomechanical Filter to Enhance the Detection Bandwidth of Gravitational-Wave Detectors. *Phys. Rev. D* **2019**, *99*, 102001. [CrossRef]
126. Korobko, M.; Ma, Y.; Chen, Y.; Schnabel, R. Quantum Expander for Gravitational-Wave Observatories. *Light. Sci. Appl.* **2019**, *8*, 118. [CrossRef]
127. Adya, V.B.; Yap, M.J.; Töyrä, D.; McRae, T.G.; Altin, P.A.; Sarre, L.K.; Meijerink, M.; Kijbunchoo, N.; Slagmolen, B.J.J.; Ward, R.L.; et al. Quantum Enhanced kHz Gravitational Wave Detector with Internal Squeezing. *Class. Quantum Gravity* **2020**, *37*, 07LT02. [CrossRef]
128. Page, M.A.; Goryachev, M.; Miao, H.; Chen, Y.; Ma, Y.; Mason, D.; Rossi, M.; Blair, C.D.; Ju, L.; Blair, D.G.; et al. Gravitational Wave Detectors with Broadband High Frequency Sensitivity. *Commun. Phys.* **2021**, *4*, 27. [CrossRef]
129. Zhang, T.; Bentley, J.; Miao, H. A Broadband Signal Recycling Scheme for Approaching the Quantum Limit from Optical Losses. *Galaxies* **2021**, *9*, 3. [CrossRef]

130. Gardner, J.W.; Yap, M.J.; Adya, V.; Chua, S.; Slagmolen, B.J.J.; McClelland, D.E. Nondegenerate Internal Squeezing: An All-Optical, Loss-Resistant Quantum Technique for Gravitational-Wave Detection. *Phys. Rev. D* **2022**, *106*, L041101. [CrossRef]
131. Wang, C.; Zhao, C.; Li, X.; Zhou, E.; Miao, H.; Chen, Y.; Ma, Y. Boosting the Sensitivity of High-Frequency Gravitational Wave Detectors Using P T-symmetry. *Phys. Rev. D* **2022**, *106*, 082002. [CrossRef]
132. Korobko, M.; Südbeck, J.; Steinlechner, S.; Schnabel, R. Mitigating Quantum Decoherence in Force Sensors by Internal Squeezing. *Phys. Rev. Lett.* **2023**, *131*, 143603. [CrossRef]
133. Korobko, M.; Südbeck, J.; Steinlechner, S.; Schnabel, R. Fundamental Sensitivity Limit of Lossy Cavity-Enhanced Interferometers with External and Internal Squeezing. *Phys. Rev. A* **2023**, *108*, 063705. [CrossRef]
134. Zhang, T.; Yang, H.; Martynov, D.; Schmidt, P.; Miao, H. Gravitational-Wave Detector for Postmerger Neutron Stars: Beyond the Quantum Loss Limit of the Fabry-Perot-Michelson Interferometer. *Phys. Rev. X* **2023**, *13*, 021019. [CrossRef]
135. Krenn, M.; Drori, Y.; Adhikari, R.X. Digital Discovery of Interferometric Gravitational Wave Detectors. *arXiv* **2023**, arXiv:2312.04258. [CrossRef]
136. Gefen, T.; Tarafder, R.; Adhikari, R.X.; Chen, Y. Quantum Precision Limits of Displacement Noise-Free Interferometers. *Phys. Rev. Lett.* **2024**, *132*, 020801. [CrossRef] [PubMed]
137. Zhao, Y.; Vardaro, M.; Capocasa, E.; Ding, J.; Guo, Y.; Lequime, M.; Barsuglia, M. Optical Losses as a Function of Beam Position on the Mirrors in a 285-m Suspended Fabry-Perot Cavity. *Phys. Rev. Appl.* **2024**, *22*, 054040. [CrossRef]
138. Demkowicz-Dobrzański, R.; Banaszek, K.; Schnabel, R. Fundamental Quantum Interferometry Bound for the Squeezed-Light-Enhanced Gravitational Wave Detector GEO 600. *Phys. Rev. A* **2013**, *88*, 41802. [CrossRef]
139. Franzen, A.; Hage, B.; DiGuglielmo, J.; Fiurášek, J.; Schnabel, R. Experimental Demonstration of Continuous Variable Purification of Squeezed States. *Phys. Rev. Lett.* **2006**, *97*, 150505. [CrossRef]
140. Dwyer, S.; Barsotti, L.; Chua, S.S.Y.; Evans, M.; Factourovich, M.; Gustafson, D.; Isogai, T.; Kawabe, K.; Khalaidovski, A.; Lam, P.K.; et al. Squeezed Quadrature Fluctuations in a Gravitational Wave Detector Using Squeezed Light. *Opt. Express* **2013**, *21*, 19047. [CrossRef]
141. Kwee, P.; Miller, J.; Isogai, T.; Barsotti, L.; Evans, M. Decoherence and Degradation of Squeezed States in Quantum Filter Cavities. *Phys. Rev. D* **2014**, *90*, 062006. [CrossRef]
142. McCuller, L.; Dwyer, S.E.; Green, A.C.; Yu, H.; Kuns, K.; Barsotti, L.; Blair, C.D.; Brown, D.D.; Effler, A.; Evans, M.; et al. LIGO's Quantum Response to Squeezed States. *Phys. Rev. D* **2021**, *104*, 062006. [CrossRef]
143. Ding, J.; Loughlin, H.A.; Sudhir, V. Quantum Linear Time-Translation-Invariant Systems: Conjugate Symplectic Structure, Uncertainty Bounds, and Tomography. *arXiv* **2024**, arXiv:2410.09976. [CrossRef]
144. Khalili, F.Y. Optimal Configurations of Filter Cavity in Future Gravitational-Wave Detectors. *Phys. Rev. D* **2010**, *81*, 122002. [CrossRef]
145. Evans, M.; Barsotti, L.; Kwee, P.; Harms, J.; Miao, H. Realistic Filter Cavities for Advanced Gravitational Wave Detectors. *Phys. Rev.-Part. Fields Gravit. Cosmol.* **2013**, *88*, 022002. [CrossRef]
146. Capocasa, E.; Barsuglia, M.; Degallaix, J.; Pinard, L.; Straniero, N.; Schnabel, R.; Somiya, K.; Aso, Y.; Tatsumi, D.; Flaminio, R. Estimation of Losses in a 300 m Filter Cavity and Quantum Noise Reduction in the KAGRA Gravitational-Wave Detector. *Phys. Rev. D* **2016**, *93*, 082004. [CrossRef]
147. Magaña-Sandoval, F.; Adhikari, R.X.; Frolov, V.; Harms, J.; Lee, J.; Sankar, S.; Saulson, P.R.; Smith, J.R. Large-Angle Scattered Light Measurements for Quantum-Noise Filter Cavity Design Studies. *J. Opt. Soc. Am. A* **2012**, *29*, 1722. [CrossRef] [PubMed]
148. Isogai, T.; Miller, J.; Kwee, P.; Barsotti, L.; Evans, M. Loss in Long-Storage-Time Optical Cavities. *Opt. Express* **2013**, *21*, 30114. [CrossRef]
149. Capocasa, E.; Guo, Y.; Eisenmann, M.; Zhao, Y.; Tomura, A.; Arai, K.; Aso, Y.; Marchiò, M.; Pinard, L.; Prat, P.; et al. Measurement of Optical Losses in a High-Finesse 300 m Filter Cavity for Broadband Quantum Noise Reduction in Gravitational-Wave Detectors. *Phys. Rev. D* **2018**, *98*, 022010. [CrossRef]
150. *pyGWINC*, version: 0.6.2; LIGO Scientific Collaboration, 2024. Available online: https://git.ligo.org/gwinc/pygwinc (accessed on 10 December 2024).
151. Töyrä, D.; Brown, D.D.; Davis, M.; Song, S.; Wormald, A.; Harms, J.; Miao, H.; Freise, A. Multi-Spatial-Mode Effects in Squeezed-Light-Enhanced Interferometric Gravitational Wave Detectors. *Phys. Rev. D* **2017**, *96*, 022006. [CrossRef]
152. Steinlechner, S.; Rohweder, N.O.; Korobko, M.; Töyrä, D.; Freise, A.; Schnabel, R. Mitigating Mode-Matching Loss in Nonclassical Laser Interferometry. *Phys. Rev. Lett.* **2018**, *121*, 263602. [CrossRef]
153. Goodwin-Jones, A.W.; Cabrita, R.; Korobko, M.; Van Beuzekom, M.; Brown, D.D.; Fafone, V.; Van Heijningen, J.; Rocchi, A.; Schiworski, M.G.; Tacca, M. Transverse Mode Control in Quantum Enhanced Interferometers: A Review and Recommendations for a New Generation. *Optica* **2024**, *11*, 273–290. [CrossRef]
154. Van Dongen, J.; Prokhorov, L.; Cooper, S.J.; Barton, M.A.; Bonilla, E.; Dooley, K.L.; Driggers, J.C.; Effler, A.; Holland, N.A.; Huddart, A.; et al. Reducing Control Noise in Gravitational Wave Detectors with Interferometric Local Damping of Suspended Optics. *Rev. Sci. Instrum.* **2023**, *94*, 054501. [CrossRef]

155. Bergamin, F.; Lough, J.; Schreiber, E.; Grote, H.; Mehmet, M.; Vahlbruch, H.; Affeldt, C.; Andric, T.; Bisht, A.; Brinkmann, M.; et al. Characterization and Evasion of Backscattered Light in the Squeezed-Light Enhanced Gravitational Wave Interferometer GEO 600. *Opt. Express* **2023**, *31*, 38443. [CrossRef] [PubMed]
156. Ma, Y.; Miao, H.; Pang, B.H.; Evans, M.; Zhao, C.; Harms, J.; Schnabel, R.; Chen, Y. Proposal for Gravitational-Wave Detection Beyond the Standard Quantum Limit via EPR Entanglement. *Nat. Phys.* **2016**, *13*, 776–780. [CrossRef]
157. Brown, D.D.; Miao, H.; Collins, C.; Mow-Lowry, C.; Töyrä, D.; Freise, A. Broadband Sensitivity Enhancement of Detuned Dual-Recycled Michelson Interferometers with EPR Entanglement. *Phys. Rev. D* **2017**, *96*, 062003. [CrossRef]
158. Beckey, J.L.; Ma, Y.; Boyer, V.; Miao, H. Broadband Quantum Noise Reduction in Future Long Baseline Gravitational-Wave Detectors via EPR Entanglement. *Phys. Rev. D* **2019**, *100*, 083011. [CrossRef]
159. Südbeck, J.; Steinlechner, S.; Korobko, M.; Schnabel, R. Demonstration of Interferometer Enhancement through Einstein–Podolsky–Rosen Entanglement. *Nat. Photonics* **2020**, *14*, 240–244. [CrossRef] [PubMed]
160. Yap, M.J.; Altin, P.; McRae, T.G.; Slagmolen, B.J.; Ward, R.L.; McClelland, D.E. Generation and Control of Frequency-Dependent Squeezing via Einstein–Podolsky–Rosen Entanglement. *Nat. Photonics* **2020**, *14*, 223–226. [CrossRef]
161. Gould, D.W.; Yap, M.J.; Adya, V.B.; Slagmolen, B.J.J.; Ward, R.L.; McClelland, D.E. Optimal Quantum Noise Cancellation with an Entangled Witness Channel. *Phys. Rev. Res.* **2021**, *3*, 043079. [CrossRef]
162. Nishino, Y.; Danilishin, S.; Enomoto, Y.; Zhang, T. Frequency-Dependent Squeezing for Gravitational-Wave Detection through Quantum Teleportation. *Phys. Rev. A* **2024**, *110*, 022601. [CrossRef]
163. Tsang, M.; Caves, C.M. Evading Quantum Mechanics: Engineering a Classical Subsystem within a Quantum Environment. *Phys. Rev. X* **2012**, *2*, 031016. [CrossRef]
164. Polzik, E.S.; Hammerer, K. Trajectories without Quantum Uncertainties. *Ann. Phys.* **2014**, *527*, A15–A20. [CrossRef]
165. Møller, C.B.; Thomas, R.A.; Vasilakis, G.; Zeuthen, E.; Tsaturyan, Y.; Balabas, M.; Jensen, K.; Schliesser, A.; Hammerer, K.; Polzik, E.S. Quantum Back-Action-evading Measurement of Motion in a Negative Mass Reference Frame. *Nature* **2017**, *547*, 191–195. [CrossRef] [PubMed]
166. Thomas, R.A.; Parniak, M.; Østfeldt, C.; Møller, C.B.; Bærentsen, C.; Tsaturyan, Y.; Schliesser, A.; Appel, J.; Zeuthen, E.; Polzik, E.S. Entanglement between Distant Macroscopic Mechanical and Spin Systems. *Nat. Phys.* **2021**, *17*, 228–233. [CrossRef]
167. Khalili, F.Y.; Polzik, E.S. Overcoming the Standard Quantum Limit in Gravitational Wave Detectors Using Spin Systems with a Negative Effective Mass. *Phys. Rev. Lett.* **2018**, *121*, 031101. [CrossRef] [PubMed]
168. Zeuthen, E.; Polzik, E.S.; Khalili, F.Y. Gravitational Wave Detection beyond the Standard Quantum Limit Using a Negative-Mass Spin System and Virtual Rigidity. *Phys. Rev. D* **2019**, *100*, 062004. [CrossRef]
169. Schönbeck, A.; Thies, F.; Schnabel, R. 13 dB Squeezed Vacuum States at 1550 Nm from 12 mW External Pump Power at 775 Nm. *Opt. Lett.* **2018**, *43*, 110. [CrossRef] [PubMed]
170. Kijbunchoo, N.; McRae, T.; Sigg, D.; Dwyer, S.E.; Yu, H.; McCuller, L.; Barsotti, L.; Blair, C.D.; Effler, A.; Evans, M.; et al. Low Phase Noise Squeezed Vacuum for Future Generation Gravitational Wave Detectors. *Class. Quantum Gravity* **2020**, *37*, 185014. [CrossRef]
171. Meylahn, F.; Willke, B.; Vahlbruch, H. Squeezed States of Light for Future Gravitational Wave Detectors at a Wavelength of 1550 Nm. *Phys. Rev. Lett.* **2022**, *129*, 121103. [CrossRef]
172. Degallaix, J. Compensation of Strong Thermal Lensing in Advanced Interferometric Gravitational Waves Detectors. Ph.D. Thesis, University of Western Australia, Perth, Australia, 2006.
173. Nadji, S.; Wittel, H.; Mukund, N.; Lough, J.; Affeldt, C.; Bergamin, F.; Brinkmann, M.; Kringel, V.; Lück, H.; Weinert, M.; et al. GEO600 Beam Splitter Thermal Compensation System: New Design and Commissioning. *arXiv* **2024**, arXiv:2408.02804. [CrossRef]
174. Whittle, C.; Hall, E.D.; Dwyer, S.; Mavalvala, N.; Sudhir, V.; Abbott, R.; Ananyeva, A.; Austin, C.; Barsotti, L.; Betzwieser, J.; et al. Approaching the Motional Ground State of a 10-Kg Object. *Science* **2021**, *372*, 1333–1336. [CrossRef]
175. Software Package "Inspiral_RANGE". Available online: https://git.ligo.org/gwinc/inspiral-range (accessed on 10 December 2024).